ASSOCIAZIONE NAZIONALE ITALIANA DI INGEGNERIA SISMICA
ANIDIS
Italian National Association of Earthquake Engineering

XVIII CONVEGNO ANIDIS
L'ingegneria sismica in Italia
ASCOLI PICENO 2019
15-19 Settembre

Comparison of approaches for generation of fully non-stationary artificial accelerograms

Piero Colajanni[a], Salvatore Pagnotta[a], Gabriele Testa[a]
[a] *Department of Engineering, Viale delle Scienze, Ed. 8, 90128 Palermo, Italy*

Keywords: Artificial accelerograms, Fully non-stationary random processes, Spectrum-compatible, RC structures

ABSTRACT
The modelling of the seismic input is a critical aspect when non-linear time-history analyses (NLTHAs) are carried out. As a matter of fact, seismic response of structures is very sensitive to the input excitation time history. The present work aims to highlight the differences in the input modelling and the assessment of seismic response of three r.c. structures employing four generation methods of fully non-stationary artificial accelerogram sets at a given construction site. For each method, seven accelerograms are generated and employed to perform NLTHAs on three r.c. structures having irregular mass and stiffness distributions. The original contribution of the paper relies in the criterion for generation method effectiveness evaluation. Efficiency is evaluated by carrying out a comparison of the structure response obtained by input modelling according to the analysed generation methods, against that evaluated by using seven recorded ground motions registered in the neighbourhood of a selected site during a same event, assumed as target accelerograms. The results point out that spectrum-compatibility based generation methods provide accelerograms able to match maximum structural displacements registered with target ground motions, but in most of them the assessed response exhibits total energy and potentially induced damage higher than that contained by the target ones. Conversely, non-spectrum-compatible method generates accelerograms having a total energy history comparable to that held by target accelerograms, but leading to wrong interstorey drift ratio assessments. The comparison claims to formulate a method of generation that combines the merits of the examined methods.

1 INTRODUCTION

The most consistent method for the seismic assessment of structures is the non-linear time-history analysis (NLTHA), which is performed using a suitable representation of the seismic input. When employing the NLTHA, the definition of appropriate accelerograms constitutes one of the source of major uncertainty, because the seismic response of structures is very sensitive to the input excitation modelling. In representing the seismicity of a given construction site, most of seismic codes (e.g. Eurocode 8) use the elastic response spectrum (RS) only, and allow the designers to use the NLTHA simply prescribing the spectrum-compatibility between the average RS of a group of accelerograms (typically seven) to be used as seismic input and the design one. Notwithstanding, RS method has the drawback of missing all the time-depending characteristics contained in accelerograms, such as duration, energy content and its time distribution, changing dominant frequency and soil damping, etc. (Rofooei et al., 2001). Thus, two accelerograms both consistent with a given target spectrum, can produce assessment of structure response characterized by different amount of dissipated energy demand and potentially induced damage, leading to a conflicting structural design in terms of resilience of elements.

In this frame, the aim of the present work is to highlight the differences in terms of assessment of seismic response of three irregular r.c. structures employing four generation methods of fully non-stationary artificial accelerogram sets at a given construction site. Few similar comparisons have been carried out in literature (e.g. Iervolino et al., 2009; Cacciola et al., 2014; Basone et al., 2017; Bianchi et al., 2018). However, in each of these works, a target code spectrum is used to apply the generation procedures, and the characteristic of the structural response obtained by the generation methods are compared among themselves, without a defined performance evaluation criterion.

In this paper, a new criterion for generation method effectiveness evaluation is proposed, based on a target input characterization and

structural response assessment defined on the basis of seven natural accelerograms with similar characteristics recorded in the neighbourhood of a selected site during the same event, named target accelerograms and target structural response. By means of these waveforms, the target spectrum is constituted, being the only information known during the generation of signals, reproducing the typical situation faced by researchers and practitioners when performing a code-consistent NLTHA. Thus, the performance evaluation criterion is chosen as the ability of reproducing the signal characteristics and the structural response assessment provided by the target set.

The reason why this work focuses only on fully non-stationary methods is because artificial accelerograms generated exploiting stationary or quasi-stationary methods have some drawbacks, such as an unrealistic amount of energy and a constant dominant frequency, which can distort the results (Li et al., 2017). At the same time, it is widely known that the non-stationary characteristics of the seismic input highly influence the dynamic response of inelastic structures (Yeh and Wen, 1990; Wang et al., 2002). The first method here employed is proposed by (Cacciola, 2010), consisting in the generation of a signal made up by two parts, a real record and a generated sample. The former is chosen in order to satisfy target site characteristics, while the latter has the aim to make the whole signal spectrum-compatible. The second method is developed by (Preumont, 1985), where accelerograms are generated by means of a modulating function both in time and frequency calibrated in order to have the same total energy of a spectrum-compatible stationary process. The third method adopted is proposed by (Rofooei et al., 2001), based on a generalized non-stationary version of the Kanai-Tajimi filter, taking into account both amplitude and frequency content variations. In order to evaluate the time-depending parameters, moving time-window technique is applied to one or more recorded earthquakes which describe the seismological conditions of the considered site. The fourth and last method is proposed by (Spanos & Solomos, 1983), in which a modulating function both in time and frequency able to reproduce the typical behavior of real earthquakes, namely a magnification of high frequency component in the early part of the sample and a dominant frequency decreasing with time, is provided. For each method, seven signals are generated and employed to perform NLTHA on three r.c. structures, having irregular mass and stiffness distributions. The investigated response parameters are interstorey drift ratios and relative storey torsional rotations. In the following section, a brief comparison between stationary and non-stationary processes is carried out, and the procedures of the four generation methods are described.

2 METHODS FOR FULLY NON-STATIONARY ACCELEROGRAMS GENERATION

Generation of artificial accelerograms is one of the most employed technique to provide seismic input to be used in NLTHAs. This technique relies on the assumption that seismic action can be associated to a sample of a Gaussian stochastic process. Mainly, three types of random processes are used to compute artificial signals: stationary, in which amplitude and frequency don't change in time, quasi-stationary (or uniformly modulated) in which only amplitude changes in time, and fully non-stationary, in which both amplitude and frequency change in time. It is well known that stationary processes lead to samples with an unrealistic amount of energy content. Furthermore, samples of ground motion generated through both stationary and quasi-stationary processes don't show the variability in dominant frequency that recorded accelerograms have. As a matter of fact, real accelerograms tend to have a changing dominant frequency due to different arrival of P- and S-wave. For these reasons, in this paper only fully non-stationary processes are used to generate samples of ground motion. According to Priestley's Evolutionary Power Spectral Density (EPSD) (Priestley, 1965), the non-stationarity in a Gaussian stochastic process can easily be obtained through the following equation:

$$G_{NST}(\omega) = |a(\omega,t)|^2 \, G_{ST}(\omega) \tag{1}$$

$G_{ST}(\omega)$ being the one-sided Power Spectral Density (PSD) of the stationary process, while $a(\omega,t)$ is the modulating function both in time and frequency. For stationary processes and given value of damping a unequivocal relationship links RS and PSD. On the other hand, removing the constraint of stationarity means dealing with an infinity of EPSDs leading to the same RS. Having said that, the focus is on how the four generation methods here analysed model the non-stationarity, by assuming that stationary PSD is obtained through only one procedure, that will be discussed here below.

2.1 Stationary model

Usually, when samples of ground motion have to be generated and employed to perform non-

linear dynamic analysis, RS is the only information given by seismic codes or known from a target event to be used as reference. Therefore, the problem is to determine the PSD through which generate samples of ground motion whose average response spectra matches the target one. In this paper, the procedure developed by (Vanmarcke and Gasparini, 1977) in the recursive form proposed by (Cacciola et al., 2004) is applied. The model highlights the correspondence between RS and PSD through the well-known "first passage problem", provided that seismic action can be reproduced by means of a zero-mean Gaussian stationary process. In detail, for a given damping ratio ζ and natural circular frequency ω, the pseudo-acceleration response spectrum RSA(ζ,ω) is linked to the mean (or median, assuming that are coincident) value of largest peak of the response of a single degree of freedom system through the equation defined as:

$$RSA(\zeta,\omega)=\omega_0^2\,\eta_U\left(\begin{matrix}T_s,p\\ \lambda_{i,U}(\omega_0,\zeta)\end{matrix}\right)\sqrt{\lambda_{0,U}(\omega_0,\zeta)} \quad (2)$$

where T_S is the time observing window duration, equal to the strong motion phase, while p is the not exceeding probability. Furthermore, under the hypothesis of a barrier outcrossing in clumps, the peak factor η_U is obtained as follows:

$$\eta_U=\sqrt{2\ln\left\{2N_U\left[1-\exp\left(-\delta_U^{1.2}\sqrt{\pi\ln(2N_U)}\right)\right]\right\}} \quad (3)$$

where the parameter N_U and the spread factor δ_U of the response process U can be approximately evaluated as:

$$N_U=\frac{T_S}{2\pi}\omega_i(-\ln p)^{-1} \quad (4)$$

$$\delta_U=\sqrt{1-\frac{1}{1-\zeta^2}\left(1-\frac{2}{\pi}\arctan\frac{\zeta}{\sqrt{1-\zeta^2}}\right)^2} \quad (5)$$

in which p = 0.5 is assumed (i.e. the mean value of the peak values). The PSD compatible with a target RS can be evaluated by means of the following expressions:

$$\begin{aligned} &G_{\ddot{u}_g}(\omega)=0 && 0\le\omega\le\omega_l\\ &G_{\ddot{u}_g}(\omega_i)=\frac{4\zeta}{\omega_i\pi-4\zeta\omega_{i-1}}\times && \\ &\times\left(\frac{RSA(\omega_i,\zeta)^2}{\eta_U^2(\omega_i,\zeta)}-\Delta\omega\sum_{j=1}^{i-1}G_{\ddot{u}_g}(\omega_j)\right) && \omega>\omega_l \end{aligned} \quad (6)$$

where ω_l is the lowest bound of the existence domain equal to 0.25 rad/s. Generally speaking, PSD obtained through the above system satisfies spectrum-compatible code provisions (e.g. Eurocode 8). Whether this is not true, the matching can be improved exploiting the following iterative scheme:

$$G_{ST}^{(j)}(\omega)=G_{ST}^{(j-1)}(\omega)\frac{RSA(\omega,\zeta)^2}{RSA^{(j-1)}(\omega,\zeta)^2} \quad (7)$$

where G^j_{ST} and $RSAj$ are the stationary PSD and the average response spectrum of the generated samples respectively, both computed at the j-th iteration. Once spectrum-compatible PSD is obtained, a sample of earthquake can be generated by means of the equation provided by (Shinozuka & Jan, 1972), superpositioning N_a harmonics with random phases:

$$\ddot{u}_g^{(k)}(t)=\sum_{i=1}^{N_a}\sqrt{2G_{\ddot{u}_g}(i\Delta\omega)\Delta\omega}\cos\left(i\Delta\omega t+\phi_i^{(k)}\right) \quad (8)$$

in which $\phi_i^{(k)}$ are phases randomly chosen in the interval [0,2π). It is noteworthy that to each sample of ground motion generated through the above procedure a second order polynomial baseline correction has to be applied in order to correct the physical unrealistic drift of velocity and displacement trajectory. In detail, each artificial accelerogram is modified by means of the procedure proposed by (Brady, 1966) as follows:

$$\ddot{\tilde{u}}_g^{(k)}(t)=\ddot{u}_g^{(k)}(t)-\left(a_0+a_1t+a_2t^2\right) \quad (9)$$

in which a_0, a_1 and a_2 are the coefficients of the polynomial to be defined in a least square sense. Once the description of the method through which define the spectrum-compatible PSD is completed, the four non-stationary methods are discussed in the next sections.

2.2 Cacciola (CA), 2010

This method models samples of earthquake via the superposition of two independent contributions: the first one is represented by a record of a real earthquake, the second one is a corrective term generated by means of a quasi-stationary zero-mean Gaussian process aiming to ensure the sample spectrum-compatibility. The advantage of the procedure is that the non-stationarity of the sample dwells in the record counterpart, which possesses all the characteristic of real earthquakes. On the contrary, the major drawback is to choose, if any and according to user's judgement, suitable records representative of the site seismological conditions. Furthermore, the chosen records should have response spectra

which fit well with the target one, in order to avoid a predominant influence of the corrective term on the overall sample. On this basis, the ground motion is given by the following equation:

$$\ddot{u}_g(t) = \alpha \ddot{u}_g^R(t) + \ddot{u}_g^S(t) \tag{10}$$

in which $\ddot{u}^R(t)$ is the record of the real earthquake, α is a scaling coefficient, while $\ddot{u}^S(t)$ is the corrective term generated through the quasi-stationary Gaussian process. Whether the RS of the recorded accelerogram is greater than the target spectrum, even if in a small range of frequencies, the coefficient α has to be taken equal to:

$$\alpha = \min\left\{\frac{RSA(\omega_i,\zeta)}{RSA^{(R)}(\omega_i,\zeta)}\right\}\left[i = 1,2.....n\right] \tag{11}$$

On the other hand, if the RS of the recorded accelerogram lies below the target spectrum, α is set equal to 1 in order to not modify the sample. Moreover, depending on the chosen record, if its RS is very small in comparison with the target one the above equation can be used to scale up the record limiting the contribution given by the artificial counterpart to the whole model. The stationary PSD is obtained through a modified version of (6):

$$G_{\ddot{u}_g}^S(\omega) = 0 \qquad 0 \le \omega \le \omega_l$$

$$G_{\ddot{u}_g}^S(\omega_i) = \frac{4\zeta}{\omega_i\pi - 4\zeta\omega_{i-1}} \times$$

$$\times U\left(\frac{RSA(\omega_i,\zeta)^2 - \alpha^2 RSA^R(\omega_i,\zeta)^2}{\eta_{U^S}^2(\omega_i,\zeta)} + \right.$$

$$\left. - \Delta\omega \sum_{j=1}^{i-1} G_{\ddot{u}_g}^S(\omega_j)\right) \times \tag{12}$$

$$\times\left(\frac{RSA(\omega_i,\zeta)^2 - \alpha^2 RSA^R(\omega_i,\zeta)^2}{\eta_{U^S}^2(\omega_i,\zeta)} + \right.$$

$$\left. - \Delta\omega \sum_{j=1}^{i-1} G_{\ddot{u}_g}^S(\omega_j)\right) \qquad \omega > \omega_l$$

in which η_{U^S}, N_U and δ_U are computed by means of (3), (4) and (5), while *U(.)* is the unit step function, added to avoid negative values of the PSD. The artificial counterpart of the whole sample is given by (8), employing PSD computed using (12). (8) is also multiplied by $\varphi(t)$, which is the modulating function in time proposed by (Jennings et al., 1969), where $t_2 - t_1 = T_S$, while β is computed as $3/(t_f - t_2)$, in which t_2 is equal to the time in which the non-stationary counterpart of the signal reaches 95% of total energy.

$$\varphi(t) = \begin{cases} \left(\frac{t}{t_1}\right)^2 & t < t_1 \\ 1 & t_1 \le t \le t_2 \\ \exp\left[-\beta(t - t_2)\right] & t > t_2 \end{cases} \tag{13}$$

The modulating function in amplitude is illustrated in Figure 1.

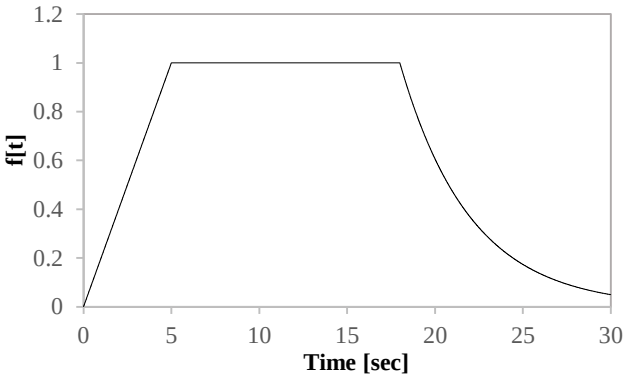

Figure 1. Modulating function in amplitude, from (Jennings et al., 1969).

To verify the spectrum-compatibility of the process, a set of 100 accelerograms is generated and the average RS is compared to the target one. Whether the code provisions are not verified, the correcting iterative scheme provided by (7) can be used until spectrum-compatibility is achieved. It is worth noting that to each artificial accelerogram is applied the baseline correction given by (9). In order to apply the method and to obtain seven different samples, an analogous number of real accelerograms are chosen, recorded during previous events than the target one in same area. These records comply with the first level seismological characteristics used to obtain the target event waveforms. It is worth to remind that the set of 100 accelerograms generated by means of the CA method is strictly spectrum-compatible, not the single sample. As a consequence, when the group of seven signals is gathered, randomly picking each sample from a different procedure, its spectrum-compatibility could not be firmly pledged.

2.3 Preumont (PR), 1985

The procedure proposed by Preumont fulfils the spectrum-compatibility requirement due to a specific type of EPSD, which reproduces the typical behavior of real accelerograms, i.e. high frequency components are amplified at the

beginning of the ground motion. The modulating function both in time and frequency that provides this characteristic is equal to:

$$\left|a\left(\omega,t\right)\right|^2 = t^2 e^{-\alpha(\omega)t} \tag{14}$$

where $\alpha(\omega)$ is a second order polynomial:

$$\alpha\left(\omega\right) = a_0 + a_1\omega + a_2\omega^2 \quad a_i \geq 0 \tag{15}$$

in which a_0, a_1 and a_2 are constants defined by users. The modulating function in amplitude and frequency is illustrated in Figure 2.

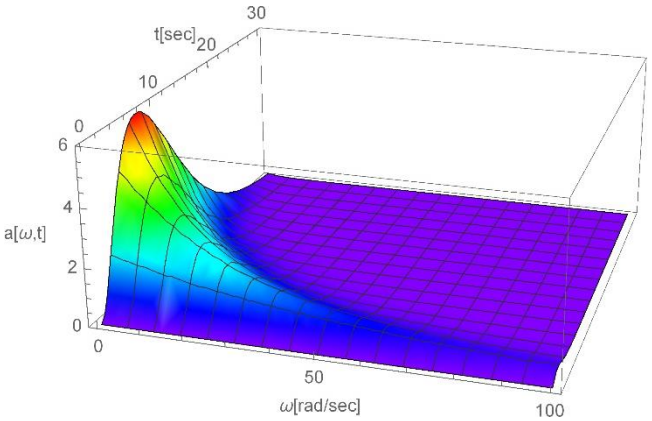

Figure 2. Modulating function both in amplitude and frequency from (Preumont, 1985).

The EPSD is given by a modified version of (1), substituting $G_{ST}(\omega)$ with $G_P(\omega)$, being a stationary PSD that ensures the spectrum-compatibility of the process, which is defined by equating, for each frequency, the energy of a quasi-stationary PSD and that of the fully non-stationary process determined by (1), as follows:

$$G_P\left(\omega\right)\int_0^\infty \left|a\left(\omega,t\right)\right|^2 dt = G_{ST}\left(\omega\right)\int_0^\infty a^2\left(t\right)dt \tag{16}$$

in which $G_{ST}(\omega)$ is a spectrum-compatible stationary PSD that can be computed by means of the previously mentioned stationary model, while $a(t)$ is a amplitude modulating function (e.g. (13)). Rearranging the previous equation, a direct correspondence between $G_P(\omega)$ and $G_{ST}(\omega)$ is found, that is:

$$G_P\left(\omega\right) = \frac{\int_0^\infty a^2\left(t\right)dt}{\int_0^\infty \left|a\left(\omega,t\right)\right|^2 dt} G_{ST}\left(\omega\right) \tag{17}$$

Once defined $G_P(\omega)$, the generation of samples of ground motion can be made using (8), employing (17) as PSD multiplied by (14) in order to model the non-stationarity. The spectrum-compatibility of the process can be checked comparing the average RS of a set of at least 100 generated accelerograms with the target one. In those rare cases the test is not satisfied, the user can use the iterative scheme given in (7), as proposed by (Cacciola & Zentner, 2012). In order to apply the method, the values of the three constants contained in (15) are chosen equal to those proposed by (Preumont, 1985), namely $a_0 = 0.3$, $a_1 = 0.01$ and $a_2 = 0$.

2.4 Rofooei, Mobarake & Ahmadi (RMA), 2001

The authors develop a model based on a generalized non-stationary version of the Kanai-Tajimi filter, taking into account both amplitude and frequency content variations. In order to evaluate the time-depending parameters, moving time-window technique is applied to one or more recorded earthquakes which describe the seismological conditions of the considered site. The model is formed by the two following equations:

$$\ddot{X}_f + 2\zeta_g\left(t\right)\omega_g\left(t\right)\dot{X}_f + \omega_g^2\left(t\right)X_f = n\left(t\right) \tag{18}$$

$$\ddot{X}_g = -\left[2\zeta_g\left(t\right)\omega_g\left(t\right)\dot{X}_f + \omega_g^2\left(t\right)X_f\right]e\left(t\right) \tag{19}$$

in which $n(t)$ is a stationary Gaussian white noise process, X_f is the filtered response, $\omega_g(t)$ is the time-varying ground frequency, $\zeta_g(t)$ is the actual soil damping, $X_g(t)$ is the artificial sample and $e(t)$ is the amplitude envelope function. As explained by the authors, the moving time-window size is defined using a trial and error method, with the purpose of choosing a suitable length long enough to guarantee a comprehensible representation of parameters, but sufficiently short to catch the quick variations in frequency content. To obtain the function $e(t)$, firstly the standard deviation within each window is calculated moving the time-window throughout the real accelerogram. Subsequently, a suitable function $\sigma_a(t)$ is defined in a least-square sense to the standard deviation values. Finally, the amplitude envelope function is found out as follows:

$$e\left(t\right) = C_0\,\sigma_a\left(t\right) \tag{20}$$

where C_0 is a constant reckoned such as a set of generated samples has the same mean energy of the target record. Differently, the ground frequency function $\omega_g(t)$ can be extracted from the number of zero-crossing rate per second using again the moving-time window, considering its size equal to the previous one. The zero-crossing rate over a generic time window is given by (21), in which t_w is the time-window size. Consequently, an appropriate function is adjusted to the zero-crossing rate trend.

$$\hat{F}_C(t) = \begin{pmatrix} Number\ of\ zero-crossing \\ within\ the\ time\ interval\left(t \pm \frac{t_w}{2}\right) \end{pmatrix} / t_w \quad (21)$$

Finally, the function $\omega_g(t)$ is determine as:

$$\omega_g(t) = \pi \hat{F}_C(t) \quad (22)$$

Despite of the chance to take into account the variability of the soil damping ratio, the authors consider it fixed imposing a suitable value. In order to apply the method, the same seven accelerograms chosen for the CA procedure are analysed. It must be emphasized that the spectrum-compatibility is not a goal of the method. At the same time, if a real ground motion has a spectrum too different to the target one, the generated samples will have this characteristic too. For this reason, the group of real samples is scaled in a least-square sense in order to have each spectrum comparable (but not spectrum-compatible) with the target one. This alteration modifies the energy amount of seismic input, not affecting the zero-crossing rate.

The paramount advantage of this method is to clearly define the ground frequency variations. On the contrary, a crucial weakness is represented by the not determined strategy to choose the soil damping ratio. To overcome this controversy, users can exploited a procedure recently proposed by (Rezaeian and Der Kiureghian, 2008) to compute the time-varying soil damping ratio. In the present work, a solution provided by (Der Kiureghian and Neuehofer, 1992) is adopted, where a fixed value of damping is given for each type of soil (e.g. firm, medium and shallow). Once determined both $\omega_g(t)$ and $\zeta_g(t)$, the following step is to generate $n(t)$, sample of a stationary Gaussian white noise process, having PSD equal to unity. Thus, by means of (18) and (19), $X_f(t)$ and $X_g(t)$ are defined using the other functions previously evaluated. Finally, the value of C_0 is defined iteratively matching the average energy of a set of 750 samples and that of the recorded ground motion.

2.5 Spanos and Solomos (SS), 1983

Among the four methods here analysed, this is the simplest one due to its easy definition of non-stationarity. As a matter of fact, the authors just propose the modulating function both in time and frequency, which is given as follows:

$$a(\omega,t) = \frac{\omega\sqrt{2}}{\alpha 5\pi} t \exp\left[-\frac{1}{2}\left(0{,}15 + \left(\frac{\omega}{\alpha 5\pi}\right)^2\right)t\right] \quad (23)$$

The modulating function (23) is illustrated in Figure 3.

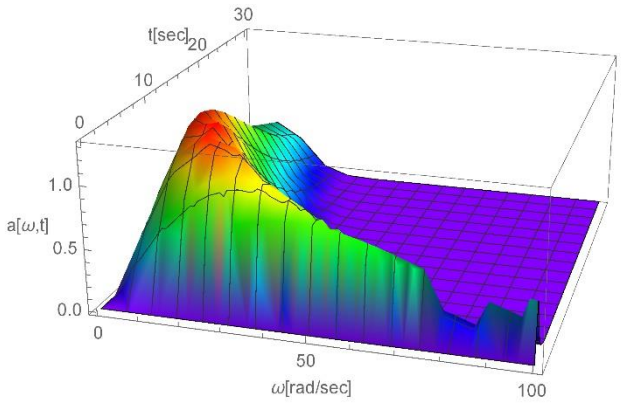

Figure 3. Modulating function both in amplitude and frequency from (Spanos and Solomos, 1983).

The parameter α is selected so that the function maximum is equal to unity, i.e. $\alpha = 3$. By so doing, it is ensured that the process remains spectrum-compatible. The modulating function allows the users to properly reproduce the typical behavior of real earthquakes, namely a magnification of high frequency component in the early part of the sample and a dominant frequency decreasing with time. At the same time, this modulating function is not able to emulate seismic inputs with different characteristics, thus its use is very limited. The generation of artificial samples is performed through (8), using (6) as PSD multiplied by the modulating function (23). If the spectrum-compatibility is not fulfilled, the iterative scheme proposed by (Cacciola, 2010) can be exploited, as done by (Basone et al., 2017), namely (7).

3 DEFINITION AND ANALYSIS OF TARGET EVENT AND SETS OF ACCELEROGRAMS

This paper aims to compare the seismic responses of structures excited by a group of seven real accelerograms which constitutes the target event, and by those obtained by four different methods for artificial accelerogram generation, assuming that, during generation of artificial ground motions, only the average response spectrum of the target event is known. Thus, it is reproduced a situation similar to that practitioners face when performing NLTHAs according to Eurocode 8 or NTC 2018, in which only the response spectrum is provided and no other indications are given. The *Engineering Strong Motion Database* (ESMD) (Luzi et al. 2016) has been used to select the target event, choosing the 6.5 M_W earthquake registered in Central Italy on 30/10/2016. The criteria through which the group of seven accelerograms has been chosen are:

- Epicentral distance *R* in the range between 15 and 40 km;
- Soil type: B;
- Peak Ground Acceleration comprised between 0.2 and 0.4 g.

It has to be underlined that both the target event and the group of seven accelerograms have been selected arbitrarily, the latter on the basis of the above-mentioned criteria. In

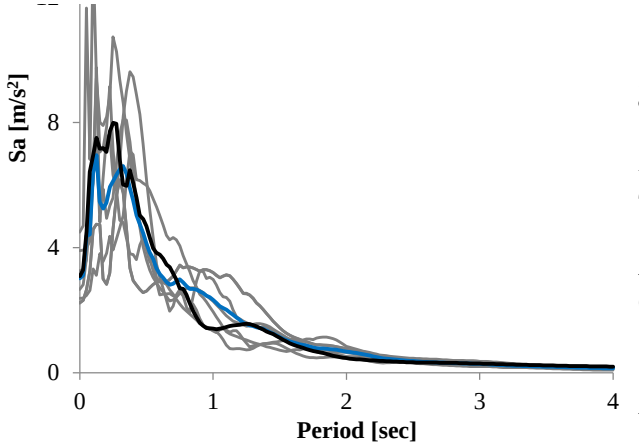

Figure 5 the response spectra and the average one of the groups of seven representative accelerograms are shown. In this figure, the accelerograms are scaled in order to have an average spectrum compatible with the target spectrum. The Event IDs, the stations where these records were recorded and the direction selected are reported in Table 1.

Table 1. Event ID, Station ID and direction of the accelerograms selected for the target and representative events.

Event ID	Station ID	Direction
Target event		
EMSC-20161030_0000029	3A.MZ10	N S
	3A.MZ63	N S
	IT.MCV	N S
	IV.T1244	E W
	IV.T1219	N S
	IV.T1220	N S
	IT.PCB	N S
Representative event		
EMSC-20161026_0000095	3A.MZ01	E W
	IV.T1201	N S
	IT.FOS	N S
	IV.T1244	E W
EMSC-20160824_0000006	IT.PCB	N S
	IT.MSCT	E W
	IT.MSC	E W

In Figures 6-9 the response spectra and the average one of the seven accelerograms generated by the four methods here employed are reported, respectively. Comparing the spectra illustrated in these figures, it can be stated that none of the method here employed is able to reproduce the variability of the seven accelerograms constituting the target event. The spectrum-compatibility between the target spectrum and those provided by the methods is Eurocode 8-compliant, namely it is checked in the range of periods between $0{,}2T_1$ and $2T_1$, where T_1 is the fundamental period of the structure in the direction where the accelerogram is applied. Moreover, no value of the mean 5% damping elastic spectrum, calculated from all time histories, is less than 90% of the corresponding value of the 5% damping elastic target spectrum. Three of the four methods (i.e.: CA, PR and SS) are developed in order to generate spectrum-compatible accelerograms. CA and SS achieves almost perfect spectrum-compatibility, while PR provides accelerograms whose spectra are 20-30% higher than the target one for periods in the range 0-0.25 sec. Conversely, RMA method generates a group of accelerograms with the highest variability among the groups here selected, but with a mean spectrum lower than the target one up to 50% in the range 0.1-0.9 sec. It is worthy to compare one of the records which constitutes the target event and one sample per method, reported in Figures 10-14, respectively. In each figure is also represented the Husid function (Husid, 1969), with the aim of understanding the distribution of the signal energy over its duration. As is well known, Husid function is defined as follows:

$$H(t)=\frac{\int_0^t\left[\ddot{u}_g(t)\right]^2}{\int_0^{t_f}\left[\ddot{u}_g(t)\right]^2} \qquad \begin{matrix} 0\le H(t)\le 1 \\ 0\le t\le t_f \end{matrix} \tag{24}$$

In (24), t_f is the total duration of the signal, while the strong motion phase is identified in the range 0,05-0,95 of *H(t)*. From the analysis of the Figures 10-14, can be stated that CA and SS methods provide waveforms dissimilar, in terms of amount of high energy cycles, to the target one, while PR and RMA methods generate signals comparable to the real one. A deep analysis reveals that CA and SS accelerograms have a strong motion phase 30% and 110% longer than that calculated in the target event signal. These outcomes are mainly due to the modulating functions in amplitude, which affect the strong motion duration of the signals. As a consequence, Husid function of CA signal has an nearly constant slope, over the strong motion phase, because of the modulating function in amplitude which is constant in the range $\approx (5 – 20)$ sec. Also the Husid function of SS signal is influenced by the modulating function, leading to a Husid function shape with a slowly decaying slope, over the strong motion phase. Conversely, PR and RMA have Husid function shapes analogous to that of the target event signal. In particular, RMA method has the advantage to

calibrate the amplitude modulating function on a recorded ground motion, that in this case is one of the signals constituting the representative accelerograms. Focusing on the frequency content

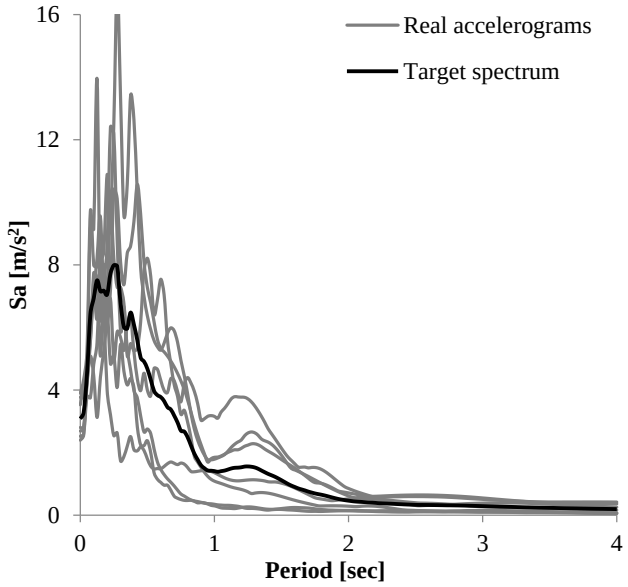

Figure 4. Response spectra and the average one of the real accelerograms representing the target event.

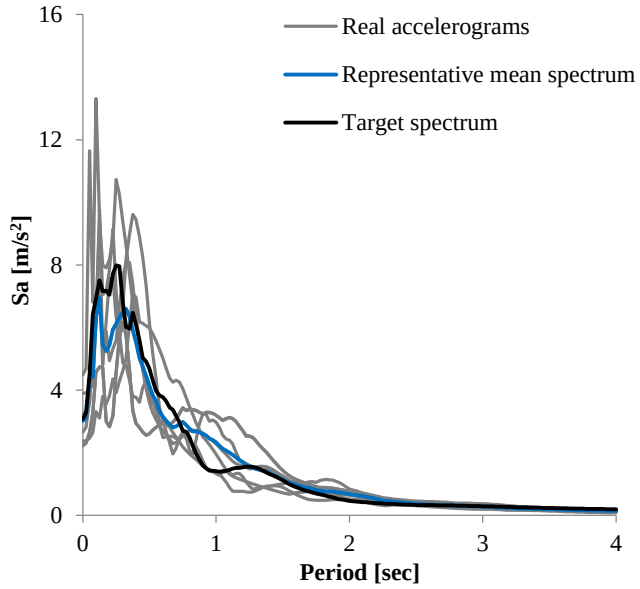

Figure 5. Response spectra and the average one of the seven representative accelerograms.

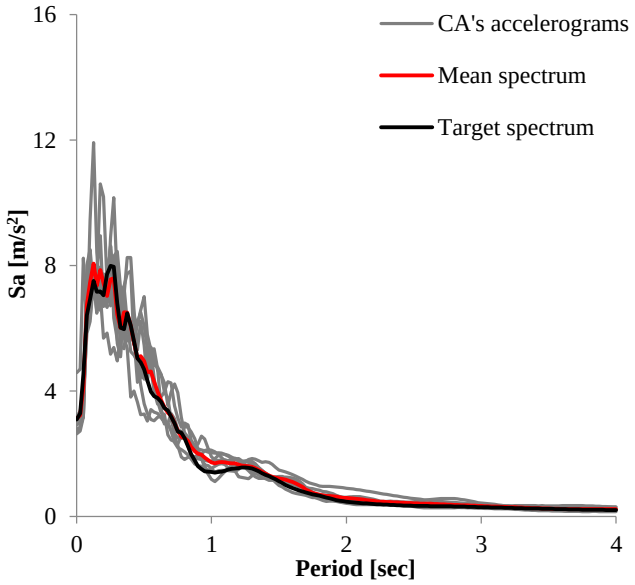

Figure 6. CA method: response spectra and the average one of the seven generated accelerograms.

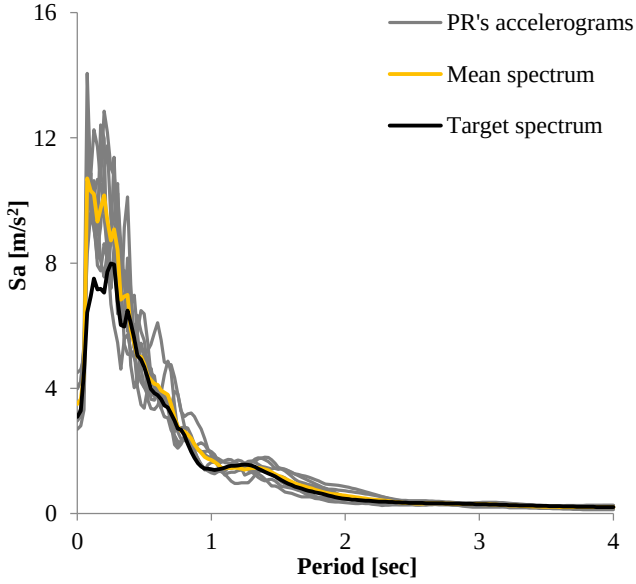

Figure 7. PR method: response spectra and the average one of the seven generated accelerograms.

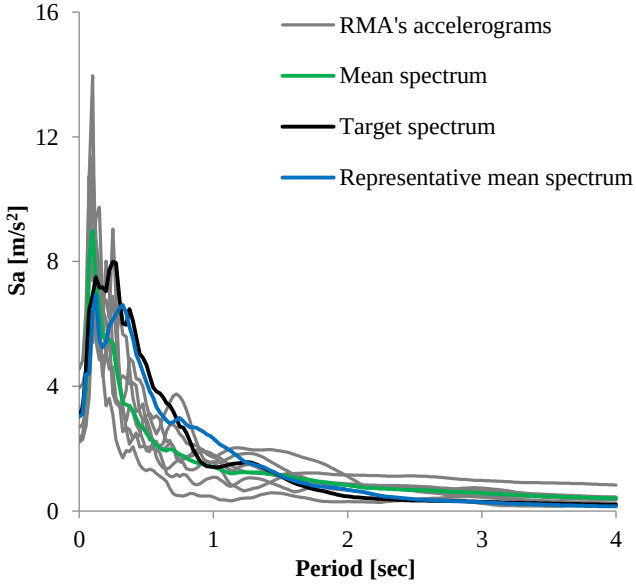

Figure 8. RMA method: response spectra and the average one of the seven generated accelerograms.

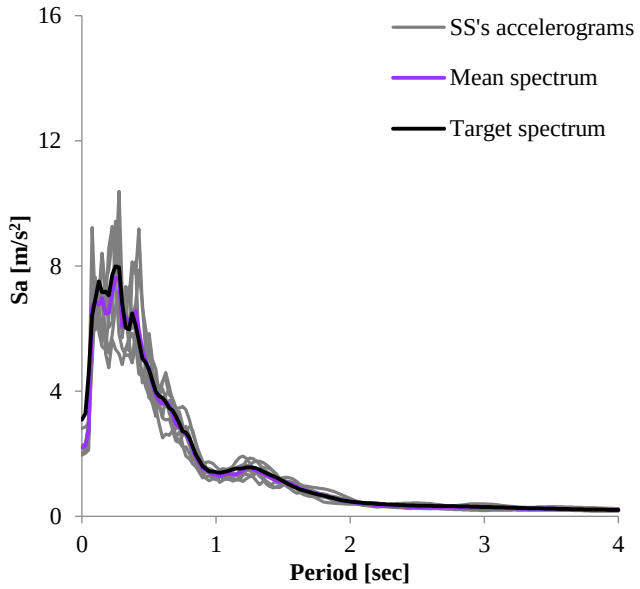

Figure 9. SS method: response spectra and the average one of the seven generated accelerograms.

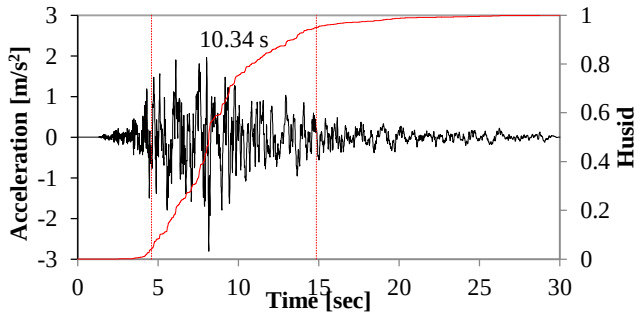

Figure 10. Acceleration time history and Husid function of one of the records constituting the target event.

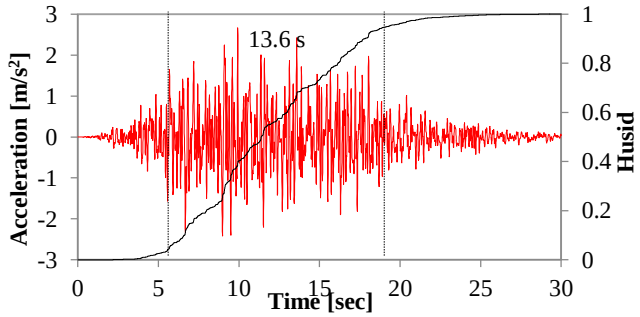

Figure 11. Acceleration time history and Husid function of one of the samples generated with CA method.

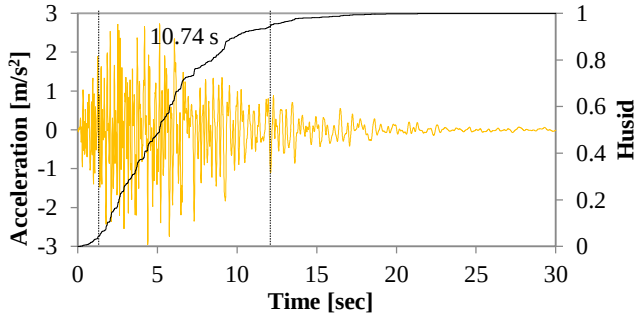

Figure 12. Acceleration time history and Husid function of one of the samples generated with PR method.

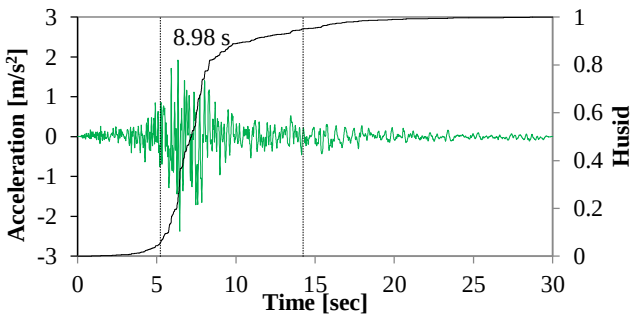

Figure 13. Acceleration time history and Husid function of one of the samples generated with RMA method.

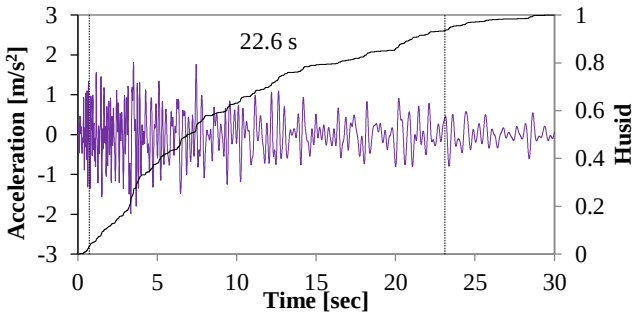

Figure 14. Acceleration time history and Husid function of one of the samples generated with SS method.

of accelerograms, PR, RMA and SS methods provide waveforms with a decaying dominant frequency over the signal duration, according to the common behavior of real record. On the other hand, CA method seems to not be able to generate accelerograms having a magnification of high frequency component in the early part of the sample and a dominant frequency decreasing with time. As a matter of fact, the CA signal has a practically constant frequency content over its duration. This phenomenon can be explained reminding (10): indeed, CA accelerogram is the sum of two contributions, the real signal, eventually scaled, and the artificial signal. In this case, in order to ensure the spectrum-compatibility of the final accelerogram, the contribution of the real signal is overshadowed by that provided by the artificial signal. For this reason, being the artificial signal generated by means of a quasi-stationary method, the non-stationarity behavior of the final accelerogram is not noticeable.

In order to clarify the characteristics of the artificial accelerograms generated by the four methods, for each signal some intensity measure parameters (IMPs) has been calculated. Thus, a comparison between IMPs of the generated and target event samples is carried out. IMPs investigated are:

- Peak Ground Acceleration (PGA);
- Peak Ground Velocity (PGV);
- Spectral Acceleration ($S_a(T_1)$), T_1=1 sec;
- Arias Intensity (I_A), proposed by (Arias, 1970), is an index representing the total amount of energy contained in a signal, and

it is computed as follows:

$$I_A = \frac{\pi}{2g}\int_0^{t_f}\left[\ddot{u}_g(t)\right]^2 dt \quad (25)$$

– Housner Intensity (I_H), proposed by (Housner, 1952), is able to describe the signal energy summing the area, contained under the Velocity Spectrum, in the range of periods 0.1-2.5 sec:

$$I_H = \int_{0.1}^{2.5} S_v\, dt \quad (26)$$

In Tables 2-6, the values of each of the above-mentioned IMPs computed for the artificial accelerograms and the target event investigated are reported. The maximum value for each group is highlighted with cyan, while the minimum with yellow. CA and RMA methods provide accelerograms with an average PGA nearly equal to the one of the target event. Conversely, CoV of RMA method is higher than the target one, while CoV of CA method is very similar to the target event. PR and SS methods seems not to be able to reproduce the average value of the PGA target, with an overestimation of 13% and an underestimation of 29%, respectively. With regard to PGV, accelerograms generated by CA and PR methods have average PGVs close to the reference value, but relative CoVs are much lower than the one of the target event. RMA method provides accelerograms with an average PGV 30% higher than the target one, while SS signals have a PGV 25% lower than the reference one. Spectral accelerations of waveforms generated by RMA method have an average value practically equal to the target one, but with a halved CoV. CA and PR methods provide signals having average spectral accelerations 20% higher than the reference value, while SS accelerograms have an average value close to the target one. It must be underlined that the spectral acceleration depends mainly on the spectrum-compatible procedure employed to generate the accelerograms, and on the degree of spectrum-compatibility demanded by the user. The results regarding the Arias Intensity highlight that none of the methods investigated is able to reproduce average I_A of accelerograms constituting the target event. Average I_A of CA, PR and SS signals are much higher than the reference one, 77%, 93% and 43% more respectively. On the other hand, RMA accelerograms has an average I_A 30% lower than the target one. CoV results reflect the procedure employed by the methods to generate accelerograms. As a matter of fact, CA,

Table 2. Peak Ground Acceleration (PGA)

	Target	CA	PR	RMA	SS
1	3.900	2.665	2.953	2.376	1.981
2	3.770	2.782	3.161	3.947	2.808
3	3.523	2.913	3.978	3.249	1.997
4	2.801	3.030	4.015	2.672	1.945
5	2.685	4.578	4.495	4.536	2.253
6	2.525	3.213	3.204	2.255	2.230
7	2.396	2.628	2.685	2.202	2.174
Avg.	3.086	3.116	3.499	3.034	2.198
CoV	20.31%	21.73%	19.00%	30.09%	13.49%

Table 3. Peak Ground Velocity (PGV)

	Target	CA	PR	RMA	SS
1	0.432	0.160	0.195	0.346	0.139
2	0.313	0.155	0.152	0.445	0.169
3	0.119	0.167	0.168	0.290	0.192
4	0.190	0.182	0.190	0.250	0.145
5	0.097	0.223	0.200	0.246	0.151
6	0.164	0.173	0.225	0.115	0.143
7	0.096	0.196	0.184	0.240	0.131
Avg.	0.202	0.180	0.188	0.276	0.153
CoV	62.57%	13.11%	12.47%	36.90%	13.78%

Table 4. Spectral Acceleration ($S_a(T_1)$)

	Target	CA	PR	RMA	SS
1	1.791	1.185	1.866	1.716	1.349
2	1.852	1.525	1.809	1.741	1.324
3	0.293	1.748	1.632	1.572	1.586
4	3.157	1.908	1.966	1.556	1.159
5	0.344	1.527	1.293	1.798	1.236
6	1.092	2.110	1.975	0.450	1.273
7	1.355	2.025	1.406	1.084	1.327
Avg.	1.412	1.718	1.707	1.417	1.322
CoV	70.10%	19.04%	15.92%	34.44%	10.10%

Table 5. Arias Intensity (I_A)

	Target	CA	PR	RMA	SS
1	1.245	1.550	1.724	0.455	1.055
2	0.868	1.427	1.439	0.748	1.345
3	0.882	1.259	1.727	0.981	1.238
4	0.785	1.881	1.831	0.763	1.245
5	0.877	1.676	2.076	0.729	1.379
6	1.231	1.603	1.780	0.329	1.304
7	0.356	1.642	1.480	0.325	1.383
Avg.	0.892	1.577	1.722	0.619	1.278
CoV	33.59%	12.46%	12.53%	40.58%	8.98%

Table 6. Housner Intensity (I_H)

	Target	CA	PR	RMA	SS
1	0.920	0.546	0.701	0.776	0.556
2	0.865	0.652	0.553	0.723	0.556
3	0.197	0.584	0.584	0.708	0.581
4	0.942	0.653	0.717	0.479	0.558
5	0.214	0.750	0.608	0.570	0.564
6	0.521	0.665	0.706	0.239	0.544
7	0.425	0.634	0.591	0.471	0.588
Avg.	0.583	0.640	0.637	0.567	0.564
CoV	55.81%	10.06%	10.76%	33.19%	2.70%

PR and SS methods adopt unchanging modulating functions, generating accelerograms which are very similar to each other. Conversely, RMA method, whose modulating functions are calibrated on real accelerograms, change for each artificial sample. Average values of Housner Intensity for RMA and SS waveforms are close to the reference one, whereas CA and PR signals overestimate the target one by 10%.

4 STRUCTURAL MODELS AND ANALYSIS OF RESULTS

The structural models used to perform the NLTHAs are three r.c. multi-storey spatial structures, with structural irregularities in elevation and plan. The software employed is (Seismostruct, 2016), in which frame elements are modelled using distributed plasticity fiber-section elements with force-based formulation. The materials constituting the structures are concrete, having a cubic compressive strength of 25 MPa, and steel with a tensile strength equal to 450 MPa. The first structure examined (Figure 15a) has a floor plan of side 10.5 x 10 m, and consists of three frames with six regular planes in height. The three frames are positioned in the x-direction parallel to the seismic input, with a distance of 5 m in the y-direction. The column stiffness distribution is symmetric (stiffness and geometric centre are coincident) while the mass distribution generate an eccentricity in the y-direction only, equal to 10% of the building transverse dimension.

The second analysed structure (Figure 15b) is irregular both in plan and elevation, having two bays in x-direction up to 4th floor and one bay in the other two floors. In this second case, beams in both x- and y-direction are 30x50 cm in size. The plan structure shows variable eccentricities between the centre of the masses and the stiffness one at the various floors. Specifically, the eccentricity values, expressed as a percentage of the building's size perpendicular to the seismic input direction, are about 15%, 10% and 5% at the first, second and third floor respectively; the last two levels are symmetric in plan.

The last building used in these numerical analyses (Figure 15c) has been designed to obtain a response heavily influenced by higher modes of vibration, especially rotational ones. As a matter of fact, in this structure the most deformable frames have been concentrated in the six-storey portion of the building, and the most rigid ones in opposite frames in the lower part of the model (4 floors) with spacing between the lower frames smaller than that between the taller ones. This configuration brings large eccentricity in all floors of the structure, leading to a magnification of the contribution of the first torsional mode to the displacement along the x-axis for the different frames. The eccentricity values, expressed as a percentage of the building's dimension perpendicular to the seismic input direction, are: 16.6%, 13.5%, and 9.25% on the first, second, and third floor, respectively; in this case also the last two levels are symmetric in plan.

Once NLTHAs have been executed, several parameters have been inspected with the aim of understanding the local and global behavior of the above-described structures. The structural damage indices (SDIs) here investigated are:

- Interstorey drift ratios (IDRs);
- Relative torsion per unit length (RT).

In Figures 17-19, considering the response to the seven signal samples for each set, the mean maximum value (MMV) and MMV ± standard deviation ranges of IDRs of the flexible side of the structures for each floor are showed. Generally speaking, it can be noticed that CA and PR waveforms tend to reproduce very well the target

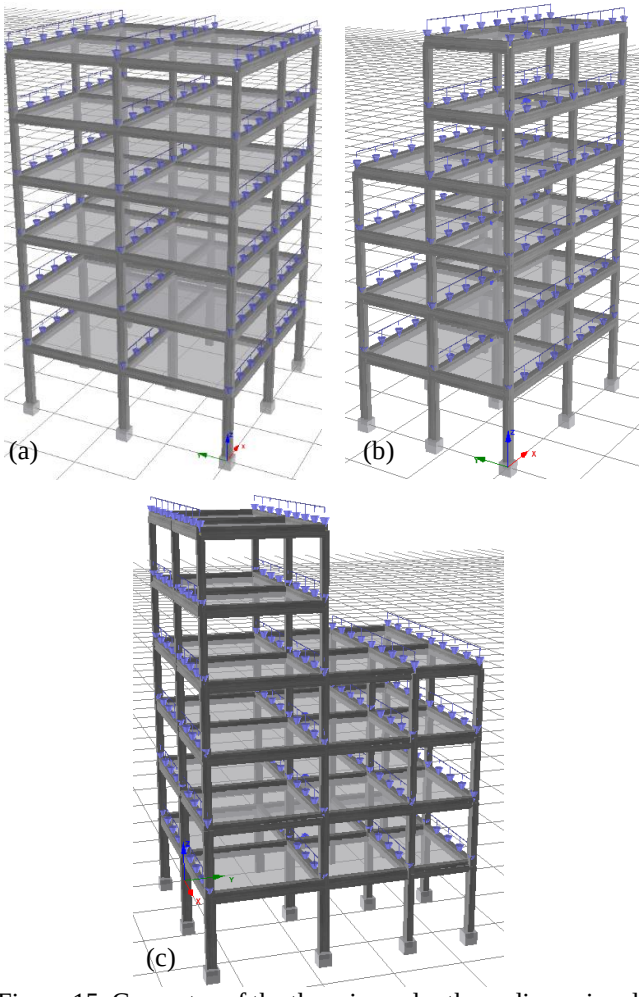

Figure 15. Geometry of the three irregular three-dimensional structures.

drift ratios, with a slight overestimation in the upper floors. On the other hand, drift ratios

obtained by SS signals are close to the target one in the upper floors, underestimating the values of the lower ones. Unreliable results are yielded by RMA accelerograms, that provides drift ratios much higher than the target ones at the lower floors, and lower at the upper ones. This phenomenon can be explained by direct inspection of RMA waveforms (Figure 13): as a matter of fact, some of the signals constituting RMA set show a pulse-like behavior, which concentrate most of the whole signal energy in few cycles, magnifying interstorey drifts at the lower floors (Tothong & Cornell, 2008). At the same time, it should be reminded that RMA method is the only one, among the four method investigated, which is not rigorously (e.g.: as Eurocode 8 prescribes) spectrum-compatible. Regarding IDR CoVs, method outcome trends are similar to those highlighted in the IMPs analysis. Indeed, PR and SS methods, whose non-stationary modulating function do not change from one sample to another, bring to accelerograms which are very similar each other. For this reason, drift ratio CoVs are limited if compared to the target ones, which

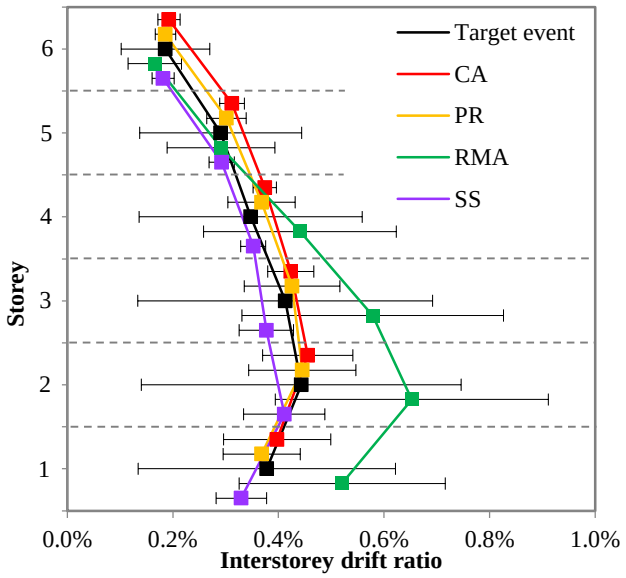

Figure 16. Structure 1: average and variability of the interstorey drift ratios.

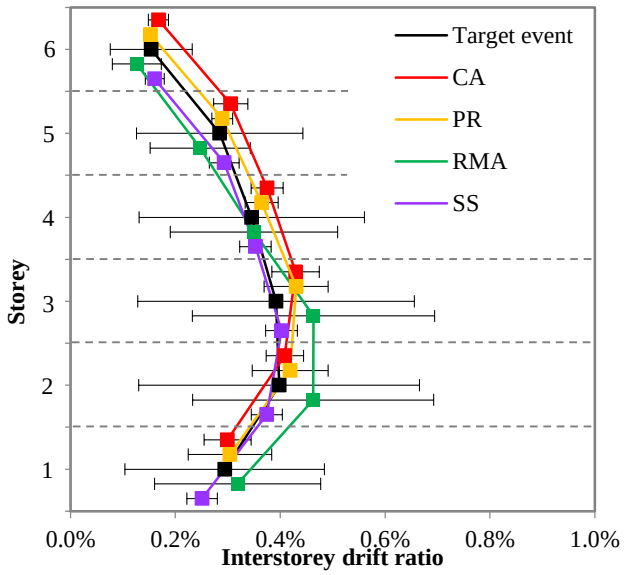

Figure 17. Structure 2: average and variability of the interstorey drift ratios.

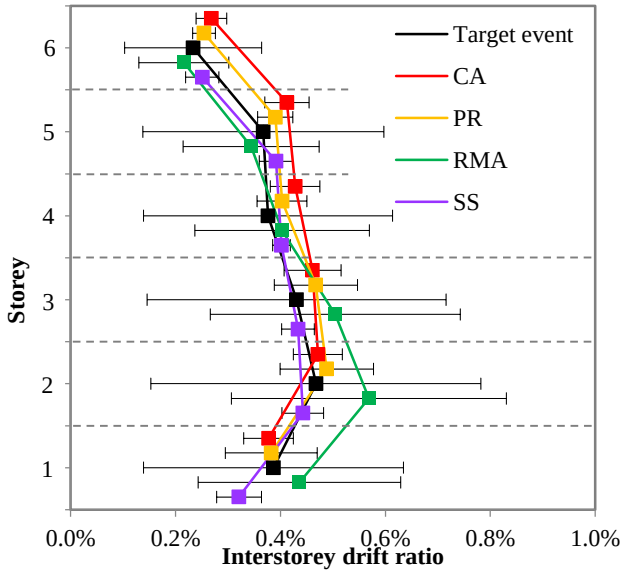

Figure 18. Structure 3: average and variability of the interstorey drift ratios.

are high in all structures. Confirming the observation on the non-stationary contribution of real accelerograms to final waveforms in CA method, drift ratio CoVs are comparable to the two aforementioned methods. By contrast, RMA signals, being generated through a non-stationary model calibrated on real records, provide IDR CoVs similar to those obtained by using target event accelerograms. Unexpectedly, observations concerning relative torsions per unit length, illustrated in Figures 20-22 for the three irregular structures, are more diversified. In fact, CA, PR and SS methods provide waveforms performing quite well in Structure 2, but they overestimate RT values in respect to the target ones in Structures 1 and 3. Vice versa, RMA accelerograms tend to underestimate RTs in the upper floors. This behavior can be clarified by looking at the energy distribution over the RMA signals.

As a matter of fact, RMA signals have an average I_A 25% lower than that held by target waveforms. Moreover, their energy is concentrated in few cycles, leading to structures whose floors tend to move contemporarily in the same direction due to the pulse-like behavior of signals. Consequently, relative torsion values tend to be smaller than the target ones. Different considerations can be developed analysing relative torsion CoVs. Overall, target and RMA accelerograms generate high CoV, consistently with their nature. On the other hand, CA, PR, and SS methods, despite generating accelerograms which are similar to one another, bring to peculiar structural behaviors. In fact, CoV values are small in those storeys in which structural irregularities are expected to less influence the structural response (e.g.: Structure 1: storeys no. 1, 5, 6; Structure 2: storeys no. 1, 2, 3, 6; Structure 3: storeys no. 1, 2, 3, 6). Conversely, CoV values are comparable to values provided by target and RMA in those storeys in which structural irregularities are concentrated (e.g.: Structure 1: storeys no. 2, 3, 4; Structure 2: storeys no. 4, 5; Structure 3: storeys no. 4, 5).

Once the results have been discussed, some considerations about the efficiency of the four methods investigated are carried out. In several studies (Akkar & Küçükdoğan, 2008; Elenas & Meskouris, 2001) have been demonstrated that PGV is highly correlated to IDR. This is confirmed by the above-described results. In fact, CA and PR signals, which are able to reproduce IDRs of the target event, have the closest average PGV to the reference value. At the same time, it is difficult to find some other correlation between IMP and SDI. As a matter of fact, only CA average PGA is comparable to the reference value, bringing acceptable results in terms of SDI. RMA signals,

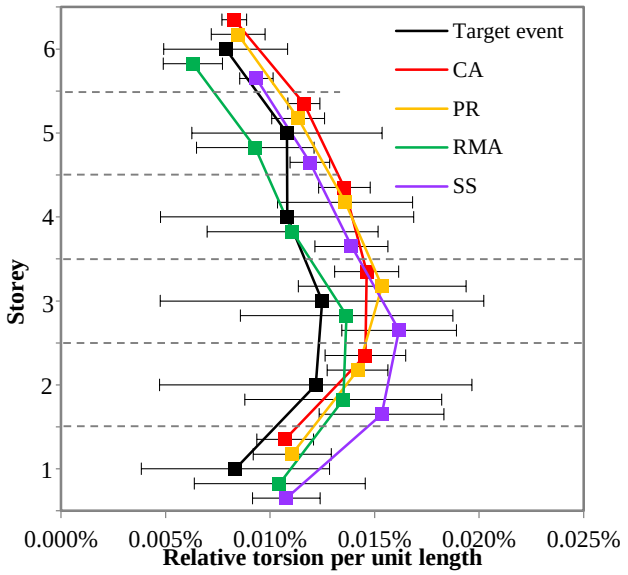

Figure 19. Structure 1: average and variability of the interstorey drift ratios.

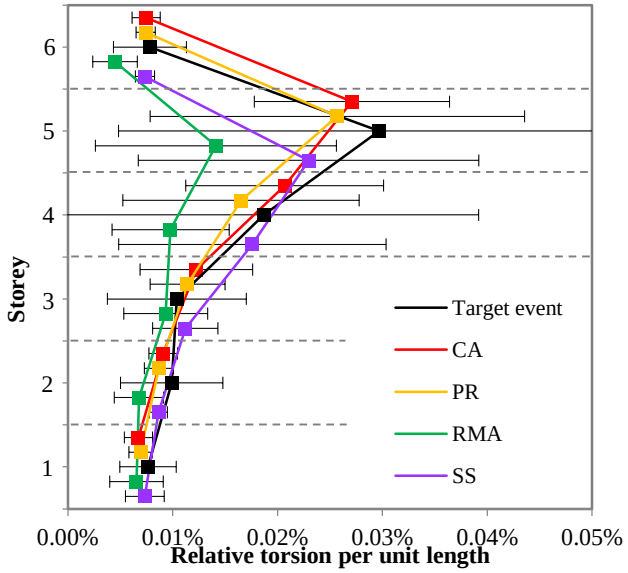

Figure 20. Structure 2: average and variability of the interstorey drift ratios.

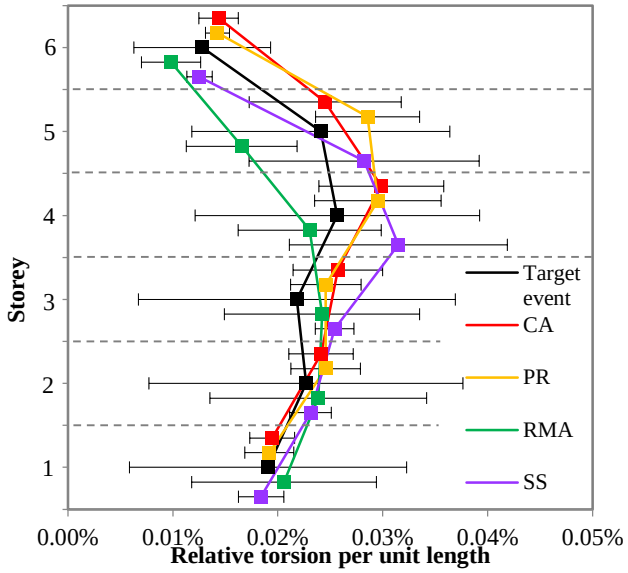

Figure 21. Structure 3: average and variability of the interstorey drift ratios.

which possess average PGA, $S_a(T_1)$ and I_H similar to the target ones, lead to the most different results compared to the reference ones.

5 CONCLUSION

In the present paper, effectiveness of four different accelerogram generation methods for fully non-stationary signals in reproducing a target event are compared. The target event has been defined, selecting seven waveforms, recorded during an earthquake in the neighbourhood of a site, that provide the target spectrum which characterizes the site seismicity. The effectiveness criteria is based on comparison of both IMPs of the generated and target signals, and results of

NLTHAs performed on three irregular r.c. structures.

It is well known that stationary and quasi-stationary signals are not able to reproduce properly the behaviour of real records. For this reason, in this work only fully non-stationary methods for generation of accelerograms have been investigated. The results pointed out some critical differences between the selected methods. First of all, none of them showed an excellent behaviour in reproducing all the Structural Damage Indexes investigated. In general terms, PR method is the one that is able to combine ease-of-use, spectrum-compatible formulation and reliable results. However, it is a challenging task to model the non-stationary characteristics of a site by means of its EPSD.

In order to perform RMA and CA methods, the seismic characteristics of a site have been represented by a group of real records, different to the target one, selected in the same site, although some issues could arise in applying this procedure in those regions where no records are available. It must be underlined that the groups of real records to be employed in CA and RMA methods are selected according to user's judgement, potentially leading to controversial results.

Despite of its rational framework, which is able to clearly define non-stationary characteristic of a site, RMA method brings the poorest results, probably due to the absence of a spectrum-compatible formulation. It should be pointed out that these results could have been affected by the few accelerograms used.

CA method provides reliable results, but they are highly influenced by the group of real records through which the non-stationary counterpart is defined. Among the methods investigated, SS method has the simplest formulation to generate signal non-stationarity, thanks to its modulating function developed in order to catch the general behavior of real records, i.e. a magnification of high frequency content at the beginning of the record and a slowly decaying predominant frequency over the duration. Conversely, it is impossible to calibrate its EPSD to site characteristics, due to its fixed modulating function. However, the results provided by the signals are acceptable, being slightly worse than those obtained through CA and PR methods.

REFERENCES

Akkar, S., Küçükdoğan, B., 2008. Direct use of PGV for estimating peak nonlinear oscillator displacement, *Earthquake Engineering & Structural Dynamics*, **37**(12), 1411-1433. DOI: 10.1002/eqe.819.

Arias, A., 1970. Measure of earthquake intensity, *Seismic Design of Nuclear Power Plants*, The MIT Press, 438-468.

Basone, F., Cavaleri, L., Di Trapani, F., Muscolino, G., 2017. Incremental dynamic based fragility assessment of reinforced concrete structures: stationary vs. non-stationary artificial ground motions, *Soil Dynamics and Earthquake Engineering*, **103**, 105-117. DOI: 10.1016/j.soildyn.2017.09.019.

Bianchi, F., Caruso, M., Lanza, A., Pinho, R., 2018. Assessing three real RC buildings using different accelerogram selection approaches, *Proc. of "16th European Conference on Earthquake Engineering"*, 18-21 June, Thessaloniki, Greece.

Brady, A.G., 1966. Studies of response to earthquake ground motion. *Dissertation (Ph.D.)*, California Institute of Technology.

Cacciola, P., Colajanni, P., Muscolino, G., 2004. Combination of modal responses consistent with seismic input representation, *Journal of Structural Engineering*, **130**(1), 47–55. DOI: 10.1061/(ASCE)0733-9445(2004)130:1(47)

Cacciola, P., 2010. A stochastic approach for generating spectrum compatible fully non-stationary earthquakes, *Computer and Structures*, **88**(15–16), 889–901. DOI: 10.1016/j.compstruc.2010.04.009

Cacciola, P., Zentner, I., 2012. Generation of response-spectrum-compatible artificial earthquake accelerograms with random joint time-frequency distributions, *Probabilistic Engineering Mechanics*, **28**, 52-58. DOI: 10.1016/j.probengmech.2011.08.004.

Cacciola, P., D'Amico, L., Zentner, I., 2014. New insights in the analysis of the structural response to response-spectrum-compatible accelerograms, *Engineering Structures*, **78**, 3-16. DOI: 10.1016/j.engstruct.2014.07.015

Der Kiureghian, A., Neuenhofer, A., 1992. Response spectrum method for multiple support seismic excitation, *Earthquake Engineering & Structural Dynamics*, **21**(8), 713–740. DOI: 10.1002/eqe.4290210805

Elenas, A., Meskouris, K., 2001. Correlation study between seismic acceleration parameters and damage indices of structures, *Engineering Structures*, **23**(6), 698-704. DOI: 10.1016/S0141-0296(00)00074-2.

Housner, G.W., 1952. Spectrum Intensities of Strong-Motion Earthquakes, *Proc. of the Symposium on Earthquake and Blast Effects on Structures*, 20-36, Los Angeles, USA.

Husid, R.L., 1969. Caracteristicas de terremotos – Analisis general, *Revista del IDEM*, **8**, 21-42, Santiago.

Iervolino, I., De Luca, F., Cosenza, E., 2009. Spectral shape-based assessment of SDOF nonlinear response to real, adjusted and artificial accelerograms, *Engineering Structures*, 3, 2776-2792. DOI: 10.1016/j.engstruct.2010.04.047.

Jennings, P.C., Housner, G.W., Tsai, C., 1969. Simulated earthquake motions for design purpose, *4th World Conference on Earthquake Engineering*, **A**(1), 145–160, Santiago, Chile.

Li, Z., Kotronis, P., Wu, H., 2017. Simplified approaches for Arias Intensity correction of synthetic accelerograms, *Bulletin of Earthquake Engineering*, **15**(10), 4067-4087. DOI: 10.1007/s10518-017-0126-6.

Luzi, L., Puglia, R., Russo, E., ORFEUS WG5 2016. Engineering Strong Motion Database, version 1.0. *Istituto Nazionale di Geofisica e Vulcanologia*,

Observatories & Research Facilities for European Seismology. DOI: 10.13127/ESM

Preumont, A., 1985. The generation of non-separable artificial earthquake accelerograms for the design of nuclear power plants, *Nuclear Engineering and Design*, **88**(1), 59–67. DOI: 10.1016/0029-5493(85)90045-7.

Priestley, M.B., 1965. Evolutionary spectra and non-stationary processes, *Journal of the Royal Statistical Society: Series B*, **27**, 204–237.

Rezaeian, S., Der Kiureghian, A., 2008. A stochastic ground motion model with separable temporal and spectral nonstationarities, *Earthquake Engineering & Structural Dynamics*, **37**, 1565-1584. DOI: 10.1002/eqe.831.

Rofooei, FR, Mobarake A, Ahmadi G (2001) Generation of artificial earthquake records with a nonstationary Kanai-Tajimi model, *Engineering Structures*, **23**(7), 827-837. DOI: 10.1016/S0141-0296(00)00093-6.

SeismoSoft. SeismoStruct – a computer program for static and dynamic nonlinear analysis of frames structures, 2016. Available at http://www.seismosoft.com.

Shinozuka, M., Jan, C.M., 1972. Digital simulation of random processes and its application, *Journal of Sound and Vibration*, **25**(1):111–128. DOI: 10.1016/0022-460X(72)90600-1.

Spanos, P., Solomos, G.P., 1983. Markov approximation to transient vibration. *Journal of Engineering Mechanics, ASCE*, **109**(4), 1134–1150. DOI: 10.1061/(ASCE)0733-9399(1983)109:4(1134).

Tothong, P., Cornell, C.A., 2008. Structural performance assessment under near-source pulse-like ground motions using advanced ground motion intensity measures, *Earthquake Engineering and Structural Dynamics*, **37**(7),1013–103. DOI: 10.1002/eqe.792

Vanmarcke, E.H., Gasparini, D.A., 1977. Simulated earthquake ground motions. *4th international conference on Smirt*, K1/9, San Francisco, USA.

Wang, J., Fan, L., Qian, S., Zhou, J., 2002. Simulations of non-stationary frequency content and its importance to seismic assessment of structures, *Earthquake Engineering and Structural Dynamics*, **31**(4), 993-1005. DOI: 10.1002/eqe.134

Yeh, C.H., Wen, Y.K., 1990. Modeling of non-stationary ground motion and analysis of inelastic structural response, *Structural Safety*, **8**(1-4), 281-298. DOI: 10.1016/0167-4730(90)90046-R